

Discrete self-similarity in interfacial hydrodynamics and the formation of iterated structures

Michael C. Dallaston¹, Marco A. Fontelos², Dmitri Tseluiko³, Serafim Kalliadasis¹

¹*Department of Chemical Engineering,
Imperial College London,
London SW7 2AZ, UK*

²*Instituto de Ciencias Matemáticas,
C/Nicolás Cabrera, Madrid, 28049, Spain*

³*Department of Mathematical Sciences,
Loughborough University,
Loughborough LE11 3TU, UK*

The formation of iterated structures, such as satellite and sub-satellite drops, filaments and bubbles, is a common feature in interfacial hydrodynamics. Here we undertake a computational and theoretical study of their origin in the case of thin films of viscous fluids subject to long-range molecular forces. We demonstrate that iterated structures appear as a consequence of discrete self-similarity, where certain patterns repeat themselves, subject to rescaling, periodically in a logarithmic time scale. The result is an infinite sequence of ridges and filaments with similarity properties. The character of these discretely self-similar solutions as the result of a Hopf bifurcation from ordinarily self-similar solutions is also described.

Free-surface flows can produce a great diversity of patterns such as filaments, drops, bubbles, pearls, waves, etc. (a review is given in [1]). Amongst them, probably the most intriguing and elusive to analyze have been the so called “iterated patterns”, i.e. “patterns within patterns” where the same structure repeats itself at different time and length scales. Such structures appear in a wide variety of physical, biological and technological settings: from natural phenomena with fractal features and structural biology to elasticity and composite materials [2]. In the context of interfacial hydrodynamics, in particular, examples of iterated structures are the formation of several generations of satellite drops in capillary breakup [3], the cascade of structures (filaments) produced in very viscous jets [4] and the iterated stretching of viscoelastic filaments [5]. In this letter, we present for the first time a scenario in which rigorous analysis reveals how such structures may appear via a bifurcation, as some structural parameter changes, from self-similar solutions to discretely self-similar ones where scale invariance occurs only at discrete times, resulting in the infinite repetition of some pattern at a discrete sequence of time and length scales.

The physical situation we consider is the rupture of thin films driven by long-range molecular forces. The forces are derived from a van der Waals-type potential. When the singularity in the potential at zero thickness is sufficiently weak, a transition between ordinary self-similarity and discrete self-similarity takes place (a general review of discrete self-similarity is given in [6]) and film rupture occurs after an infinite sequence of droplets is produced.

Thin liquid films are ubiquitous in a wide spectrum of natural phenomena and technological applications [7]. When the film thickness is sufficiently small, molecular

forces play an important role and may cause the film to destabilize and eventually rupture and dewet the substrate. In the long-wave approximation (the interface slope is small, as is appropriate for slow flows with strong surface tension) the problem may be formulated in terms of an evolution equation for the film profile $h(\mathbf{x}, t)$ in the form $h_t = -\nabla \cdot \mathbf{q}$, where $\mathbf{q} = -(h^3/3\mu)\nabla p$ is the flow rate, with μ being the fluid’s viscosity, and the pressure p has two contributions:

$$-p = \sigma \nabla^2 h + \Pi(h).$$

The first component is the usual Laplace pressure (linearized curvature times surface tension coefficient) and the second is the disjoining pressure taken to be of the form

$$\Pi(h) = -\frac{A}{h^n}.$$

In one spatial dimension, and after a suitable nondimensionalization, the model for the evolution of a thin liquid film under the action of molecular forces then reads

$$h_t + \left[h^3 \left(h_{xx} - \frac{1}{nh^n} \right) \right]_x = 0. \quad (1)$$

In the context of rupture by van der Waals forces, A (strictly, $6\pi A$) is the Hamaker constant, while the exponent is almost always taken to be $n = 3$ [8, 9], consistent also with elements from statistical mechanics of fluids, namely density-functional theory (DFT), where the disjoining pressure with $n = 3$ is an asymptote to DFT as the distance of the chemical potential from saturation vanishes, assuming a Lennard–Jones potential for pairwise molecular interactions and neglecting screening effects [10].

At $n = 3$, the remarkable property of solutions of (1) is the development of self-similar film rupture ($h = 0$ at a single point) in finite time [8, 9]. There is, however, good reason to examine different values of n . A great deal of experimental study has shown that the functional form of the disjoining pressure is highly dependent on the nature of the dominant intermolecular force, which in turn is influenced by the substrate and liquid properties. For example, [11] found that the effects of screening can lead to a potential better modeled with $n = 4$ in hydrocarbon-metal experiments where the film was of thickness > 40 nm, while the contribution due to hydrogen bonding in water-quartz experiments for very thin (~ 10 nm) films was better approximated by $n = 1$ [12]. A good summary of different contributions to the disjoining pressure may be found in [13]. The dynamics of rupture under these different values has not previously been examined.

As well as intermolecular forces, the above formulation is used to model other thin-film phenomena at different scales, such as destabilization of thin films due to thermocapillarity [14] and density contrast (Rayleigh–Taylor instability) [15]; in such cases we may define an equivalent “disjoining pressure”, which behaves as $\Pi(h) \sim \ln(h)$ for the thermocapillary effect (essentially $n = 0$), or $\Pi(h) \sim h$ for the Rayleigh–Taylor instability ($n = -1$). Instead of self-similar rupture, these two examples exhibit cascades of satellite droplets, similar to those discussed above, so it is of great interest to understand how the two behaviors are connected through variation in n .

Assuming that rupture occurs at a single point x_0 and at time t_0 , it is natural to seek solutions in a self-similar form:

$$h(x, t) = (t_0 - t)^\alpha f \left(\xi \equiv \frac{x - x_0}{(t_0 - t)^\beta} \right), \quad (2)$$

where, from simple dimensional arguments based on (1), one finds the following values for the similarity exponents α and β :

$$\alpha = \frac{1}{2n - 1}, \quad \beta = \frac{n + 1}{4n - 2}. \quad (3)$$

In order for a self-similar solution representing rupture to exist, we must assume $n > 1/2$, so that α and β are positive. The self-similar solution $f(\xi)$ must then satisfy the equation

$$-\frac{1}{2n - 1}f + \frac{n + 1}{4n - 2}\xi f_\xi + \left[f^3 \left(f_{\xi\xi} - \frac{1}{nf^n} \right) \right]_\xi = 0, \quad (4)$$

subject to the condition that the interface profile $h(x, t)$ remains finite at a finite distance from x_0 . As $t \rightarrow t_0$, one has $\xi \rightarrow \infty$ and, in order to cancel out any dependence on $t_0 - t$ we must impose

$$f(\xi) \sim C_\pm |\xi|^{\alpha/\beta} = C_\pm |\xi|^{2/(n+1)} \quad \text{as } |\xi| \rightarrow \infty, \quad (5)$$

where C_\pm are constants as $\xi \rightarrow \pm\infty$.

Above a certain value of n , there are an infinite number of solutions to (2) with boundary condition (5). This fact was established for the particular case $n = 3$ in [8] and was recently extended to general n by the authors [16]. These solutions are symmetric, that is, $C_+ = C_-$, and can be arranged (for a given value of n) as a sequence f_1, f_2, f_3, \dots according to their values at $\xi = 0$ such that $f_1(0) > f_2(0) > \dots$. We can thus depict solution branches as $f_j(0)$ over n (Fig. 1). These solutions were computed using the open source numerical continuation software AUTO-07p [17] (see also [16, 18]). As n is decreased, the solution branches merge, with the first two branches merging at the critical value $n_c = 1.49915$ [16]. Our focus in this letter is on the change in dynamics of solutions to (1) close to this value.

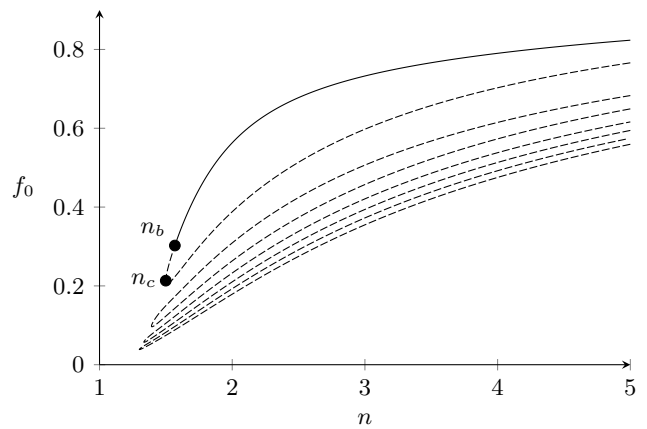


FIG. 1. Bifurcation diagram for self-similar solutions $f(\xi)$ satisfying (4), labelled by their value at the origin $f_0 = f(0)$. For sufficiently large n , there are infinitely many solutions. At $n = n_c \simeq 1.49915$ there is a first turning point where the first and second branches of solutions merge. Successive turning points exist at 1.39141, 1.33405, 1.29993, \dots . The primary branch is stable for most of its domain; however, as we describe in this letter, it becomes unstable below $n = n_b$ due to a Hopf bifurcation there (see Fig. 4).

To compute numerical solutions to (1), we implement an adaptive finite difference scheme that increases local mesh refinement near the minimum of h whenever h_{\min} is less than half of its value at the previous mesh refinement. In Fig. 2(a), we represent the result of such a computation with $n = 1.7$, as well as a comparison of the numerical profiles rescaled according to (2) with the self-similar solution $f_1(\xi)$. At this value of n , the solution ruptures in finite time t_0 . If we solve (1) with $n = 1.4$ instead [Fig. 2(b)], the situation changes dramatically; there is still finite-time rupture at a single point, but the approach is not in the form (2) anymore, with the solution instead developing an infinite cascade of satellites of decreasing size at $x > x_0$ and at $x < x_0$.

The existence of these spatial and temporal oscillations at $n = 1.4$ indicates discretely self-similar (DSS) solu-

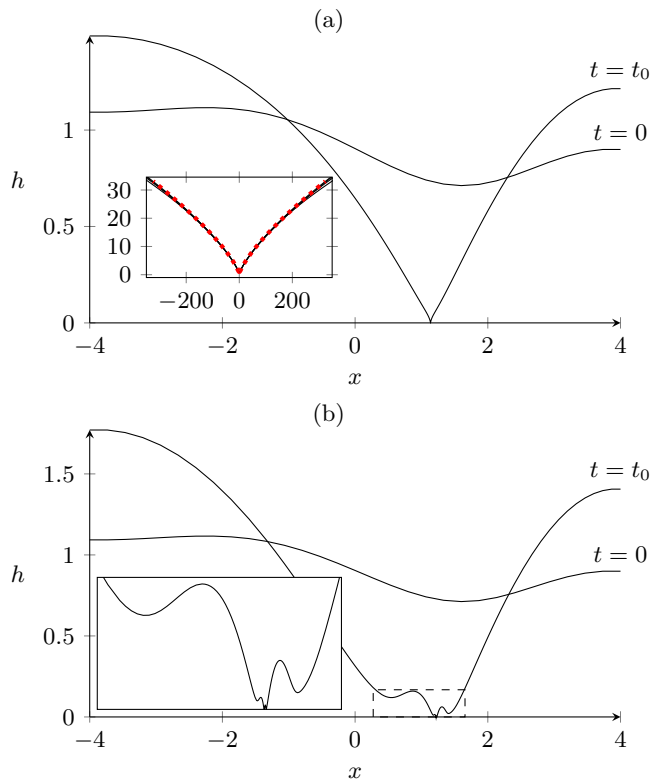


FIG. 2. (a) Evolution towards rupture in the domain $[-L, L]$, $L = 4$, with the initial profile $h(x, 0) = 1 - (1/10) \cos(\pi x/2L) - (1/5) \sin(\pi x/L)$ and $n = 1.7$. Rupture occurs at a point at time $t = t_0$. Inset: Interface profiles near the singularity rescaled according to (2), and comparison with the stable self-similar solution (dotted line). The interface profiles approach a symmetric self-similar shape, even though the initial profile is asymmetric. (b) Evolution from the same initial condition, but with $n = 1.4$. Rupture occurs at a point at time $t = t_0$. In this case, the evolution is not of the classical self-similar type. Inset: a magnification of the region inside the dashed rectangle in the main figure shows progressively smaller oscillations.

tions (general references on DSS and its role in various physical systems are given in [19]). For these solutions, the relationship (2) holds only for a discrete family of times t_1, t_2, \dots , which approach t_0 exponentially. As argued in [6], DSS solutions appear as periodic orbits when writing (2) in the natural self-similar variables. More precisely, we perform the change of variables:

$$h(x, t) = (t_0 - t)^\alpha F \left(\tau = -\log(t_0 - t), \xi \equiv \frac{x - x_0}{(t_0 - t)^\beta} \right) \quad (6)$$

so that (1) with α, β given by (3) transforms into the equation:

$$F_\tau - \frac{1}{2n-1} F + \frac{n+1}{4n-2} \xi F_\xi + \left[F^3 \left(F_{\xi\xi} - \frac{1}{nF^n} \right) \right]_\xi = 0. \quad (7)$$

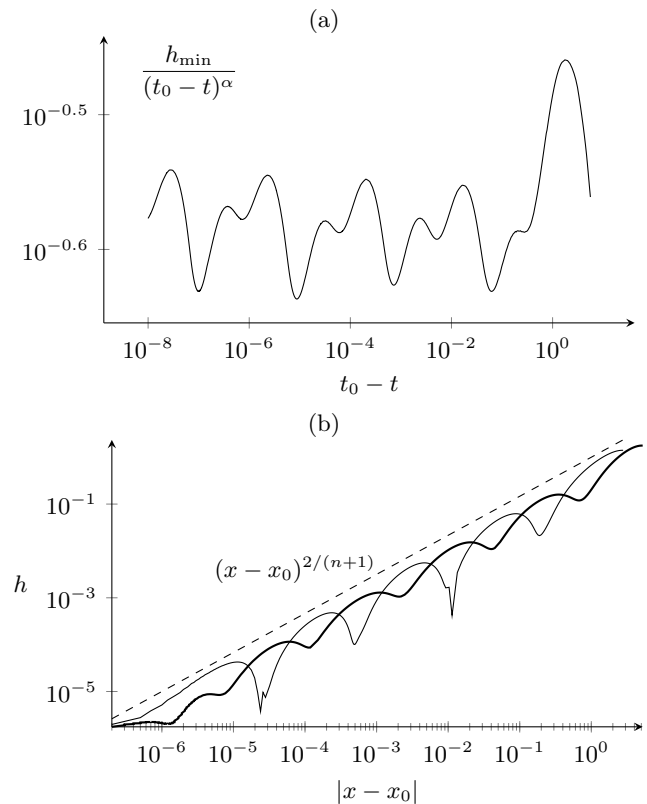


FIG. 3. (a) Logarithmic plot of the minimum interface height h_{\min} divided by the assumed similarity scaling $(t_0 - t)^\alpha$, against time to the singularity $t_0 - t$. On average, h_{\min} is dictated by the scaling, but also exhibits periodic oscillations that are characteristic of discrete self-similarity. We have computed four complete periods. (b) Logarithmic plot of the interface shape against distance to the point of rupture x_0 close to time t_0 . The two branches correspond to $x > x_0$ (unbolded line) and $x < x_0$ (bolded line). On average, the slope is dictated by scaling (dashed line), but large periodic oscillations are observed, corresponding to sequences of ridges and necks.

The scaled time variable τ tends to infinity as $t \rightarrow t_0$. Self-similar solutions f_1, f_2, \dots of (4) are fixed/ equilibrium points (that is, τ -independent) of (7) viewed as a dynamical system in the scaled time τ . Hence, for a given value of n , $\{f_1(\xi), f_2(\xi), f_3(\xi), \dots\}$ is the set of equilibrium points in the dynamics. Besides equilibrium points, other attractors such as periodic orbits may be present. A periodic orbit of period T is characterized by the property $F(\tau + T, \xi) = F(\tau, \xi)$ for any value of τ . Thus, the same profile $(x - x_0, h)$, up to rescaling both coordinates with $(t_0 - t)^\beta$ and $(t_0 - t)^\alpha$ respectively, will appear at times $t_1, t_2, \dots, t_N, \dots$ such that

$$\frac{t_0 - t_{N+1}}{t_0 - t_N} = e^{-T}. \quad (8)$$

From our numerical solution of the evolution of (1) for $n = 1.7$ and $n = 1.4$ in Fig. 2, it is clear that the nature of the self-similarity changes significantly between these two

values. We will now argue that attracting periodic orbits occur when n is smaller than a critical value $n_b \simeq 1.576$, strictly larger than the value n_c at which the first two branches merge.

As the first evidence for a periodic behavior, in Fig. 3 we depict the evolution of the minimum interface height $h_{\min}(t)$ in a logarithmic scale for a full numerical simulation of (2) with $n = 1.4$. In the case of a self-similar solution in the form (2), one would have $h_{\min} \sim f_0(t_0 - t)^\alpha$. In the case of a DSS solution, the minimum in ξ of F is achieved at a point $\xi_0(\tau)$ changing periodically in τ , and hence we have $h_{\min} = F(\tau, \xi_0(\tau))(t_0 - t)^{-\alpha}$. On a logarithmic scale this relation is a superposition of a straight line of slope $-\alpha$ and a periodic function in τ . In Fig. 3 we plot h_{\min} divided by $(t_0 - t)^\alpha$ against $t_0 - t$ on a logarithmic scale. The periodicity can be clearly seen, and we resolve h_{\min} down to 10^{-8} , which covers four full periods. From these numerics we estimate the period to be $T \simeq 4.6$.

Secondly, in Fig. 3b we plot h against $|x - x_0|$, on a logarithmic scale, for t very close to t_0 . In the case of self-similar rupture, the far field condition of f (5) sets the power law behaviour of the film profile near rupture to be $h \sim C_\pm |x - x_0|^{2/(n+1)}$. For a DSS solution, the far field of f oscillates in scaled time τ , which leaves behind a pattern of local maxima and minima, whose amplitude and spacing decrease exponentially as the rupture point x_0 is approached. The local maxima can be interpreted as crests of “drops” and the local minima as necks separating the drops. The maxima $h_1, h_2, \dots, h_N, \dots$ are located at distances $d_1, d_2, \dots, d_N, \dots$ from x_0 . The distances d_i correspond to identical values of $\xi = d_i(t_0 - t_i)^{-\beta}$ and the heights h_i correspond to identical values of $f = h_i(t_0 - t_i)^{-\alpha}$, at times t_i satisfying (8). Hence, from (6) we deduce

$$\frac{d_N}{d_{N+1}} = e^{\beta T}, \quad \frac{h_N}{h_{N+1}} = e^{\alpha T}.$$

These predicted values are accurately reflected in the numerical result in Fig. 3.

A theoretical understanding of self-similar dynamics requires the computation of not only the equilibrium points but also their (linear) stability. For $n = 3$ it has been shown [9] that besides two trivial eigenvalues that correspond to space and time translation of the singularity [6], all eigenvalues of the linearization of (7) about $f_1(\xi)$ are negative. Hence, the similarity solution $f_1(\xi)$ is a stable equilibrium point. $f_2(\xi)$, on the other hand, has one positive nontrivial eigenvalue and $f_3(\xi)$ has two nontrivial eigenvalues, etc. All equilibrium points other than $f_1(\xi)$ are therefore unstable.

We now compute the stability of $f_1(\xi)$ as n varies. This is again carried out using AUTO-07p [17]. We linearize equation (7) about $f_1(\xi)$ and seek solutions of the linearized problem in the form $\tilde{f}(\tau, \xi) = e^{\sigma\tau}\Phi(\xi)$, which

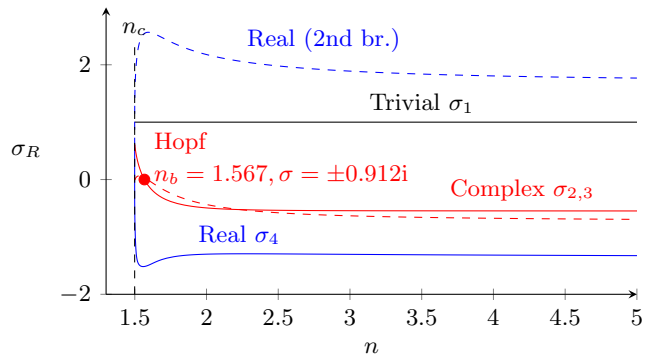


FIG. 4. The real part σ_R of eigenvalues governing the stability of the primary solution branch $f_1(\xi)$ as n varies (solid), and eigenvalues of the second branch $f_2(\xi)$ (dashed). The real part of the complex eigenvalues $\sigma_{2,3}$ crosses zero at $n_b \simeq 1.567$, indicating a Hopf bifurcation.

leads to an eigenvalue problem for σ . For complex eigenvalues we write $\sigma = \sigma_R + i\sigma_I$.

The four eigenvalues $\{\sigma_j\}$ with largest real part are represented in Fig. 4. The largest is $\sigma_1 = 1$, which is the trivial eigenvalue corresponding to changes in t_0 (the eigenvalue arising from a perturbation in x_0 is suppressed by the assumed symmetry). The pair $\sigma_{2,3}$ are complex conjugates that result from the collision of two real eigenvalues at a point $n > 5$. At a critical value $n = n_b \simeq 1.567 > n_c$, the real part $\sigma_{R2,3}$ of this complex pair crosses from negative to positive; hence, as n decreases, the stable focus $f_1(\xi)$ switches into an unstable focus which results in a periodic orbit via a Hopf bifurcation. The imaginary part of the eigenvalue $\sigma_{I2,3}$ at $n = n_b$ sets the frequency of oscillations of the periodic orbits as $n \rightarrow n_b^-$ and of damped oscillations about $f_1(\xi)$ as $n \rightarrow n_b^+$. We find this value to be $\sigma_I \simeq \pm 0.9125$. Finally, σ_4 is the largest nontrivial real eigenvalue, which plays a role in the fold bifurcation at $n = n_c$ where the first and second branches merge. The nature of the fold bifurcation is quite subtle, and appears to be a Bogdanov–Takens (double zero) singularity [20], although we do not go into greater detail in this letter.

A natural question is whether further bifurcations take place at smaller values of n , leading to more complicated dynamics. We considered the particular case $n = 0.7$ which is far from n_c but still above $n = 1/2$. As is evident from Fig. 5, the minimum height roughly evolves according to the similarity scaling, but the oscillation around the similarity exponent does not show any periodicity. This translates into a chaotic distribution of drops near $t = t_0$ without any clear pattern. It is noteworthy that recently, the transition from stable self-similar to chaotic behavior has also been observed in the context of slip instabilities in elasticity [in particular, simulations of the frictional sliding dynamics of two elastic bodies in contact [21], in which there is a series of Hopf bifurcations

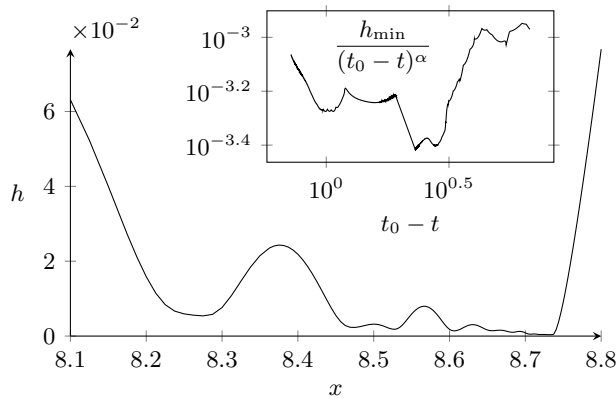


FIG. 5. Interface profile for $n = 0.7$ and t close to t_0 . No regular pattern can be observed. Inset: logarithmic plot of the minimum height, divided by the appropriate similarity scaling, against time to the singularity. Note the apparent chaos without a clearly defined pattern.

(instead of the single one that our system exhibits) on the branch of steady (self-similar) states] but as far as we are aware Eq. (1) is the first PDE model in hydrodynamics in which a limit cycle in self-similar variables appears and which subsequently leads to chaotic dynamics.

It is also noteworthy that previous studies on thermocapillary and Rayleigh–Taylor instability, which have equivalent disjoining pressures with values $n < 1/2$, show that the formation of smaller and smaller drops occurs through a process that appears chaotic, and this behavior is also exhibited when the system is modeled with the full Stokes or Navier–Stokes equations [14, 15]. The transition from finite-time self-similar rupture to DSS, and then to chaotic behavior, is therefore of true physical interest in the study of interfacial phenomena and is worth further theoretical investigation.

We acknowledge financial support from the Engineering and Physical Sciences Research Council (EPSRC) of the UK through Grants No. EP/K008595/1 and EP/L020564/1. The work of DT was partly supported by the EPSRC through Grant No. EP/K041134/1.

-
- [1] J. Eggers and E. Villermaux, Rep. Prog. Phys. **71**, 1 (2008).
 [2] B. B. Mandelbrot, *The Fractal Geometry of Nature* (Macmillan, 1983); A. Perrakis, R. Morris, and V.S. Lamzin, Nat. Struct. Mol. Biol. **6**, 458 (1999); D. Lukkassen, SIAM J. Appl. Math. **59**, 1825 (2006).

- [3] M. Tjahjadi, H. A. Stone, and J.M. Ottino, J. Fluid Mech. **243**, 297 (1992).
 [4] X. D. Shi, M. P. Brenner, and S. R. Nagel, Science **265**, 219 (1994); M. P. Brenner, X. D. Shi, and S. R. Nagel, Phys. Rev. Lett. **73**, 3391 (1994).
 [5] H.-C. Chang, E. A. Demekhin, and E. Kalaidin, Phys. Fluids **11**, 1717 (1999); M. S. N. Oliveira and G. H. McKinley, Phys. Fluids **17**, 071704 (2005).
 [6] J. Eggers and M. A. Fontelos, *Singularities: Formation, Structure, and Propagation* (Cambridge University Press, 2015).
 [7] R. V. Craster and O. K. Matar, Rev. Mod. Phys. **81** 1131 (2009).
 [8] W. W. Zhang and J. R. Lister, Phys. Fluids **11**, 2454 (1999).
 [9] T. P. Witelski and A. J. Bernoff, Phys. Fluids, **11**, 2443 (1999); T. P. Witelski and A. J. Bernoff, Physica D **147**, 155 (2000).
 [10] P. Yatsyshin, N. Savva, and S. Kalliadasis, J. Chem. Phys. **142**, 034708 (2015); S. Dietrich and M. Napióórski, Phys. Rev. A **43**, 1861 (1991); A. González and M. M. Telo da Gama, Phys. Rev. E **62**, 6571 (2000).
 [11] B. V. Derjaguin and N. V. Churaev, J. Coll. Interf. Sci. **49**, 249 (1974).
 [12] R. M. Pashley, J. Coll. Interf. Sci. **78**, 246 (1980).
 [13] G. F. Teletzke, H. T. Davis, and L. E. Scriven, Rev. Phys. Appl. **23**, 989 (1988). G. F. Teletzke, H. T. Davis, and L. E. Scriven, Chem. Eng. Commun. **55**, 41 (1987);
 [14] W. Boos and A. Thess, Phys. Fluids **11**, 1484 (1999); A. Alexeev, T. Gambaryan-Roisman, and P. Stephan, Phys. Fluids **17**, 062106 (2005); S. Krishnamoorthy, B. Ramaswamy, and S. W. Joo, Phys. Fluids **26**, 072001 (2014).
 [15] S. G. Yiantsios and B. G. Higgins, Phys. Fluids A **1**, 1484 (1989).
 [16] M. C. Dallaston, D. Tseluiko, Z. Zheng, M. A. Fontelos, and S. Kalliadasis, Self-similar finite-time singularity formation in degenerate parabolic equations arising in thin-film flows, arXiv:1609.03913 (2016).
 [17] E. J. Doedel, A. R. Champneys, F. Dercole, T. F. Fairgrieve, Y. A. Kuznetsov, B. Oldeman, R. C. Paffenroth, B. Sandstede, X. J. Wang, and C. H. Zhang, *AUTO-07p, Continuation and bifurcation software for ordinary differential equations*, <http://indy.cs.concordia.ca/auto/> (2007).
 [18] D. Tseluiko, J. Baxter, and U. Thiele, IMA J. Appl. Math. **78**, 762 (2013).
 [19] D. Sornette, Physics Reports **297**, 239(1998); D. Sornette, *Critical Phenomena in Natural Sciences: Chaos, Fractals, Self-Organization and Disorder: Concepts and Tools* (Springer Science & Business Media 2006).
 [20] Y. A. Kuznetsov, *Elements of Applied Bifurcation Theory*, **112** (Springer Science & Business Media 2013).
 [21] R. C. Viesca, Proc. R. Soc. A **472**, 20160254 (2016); R. C. Viesca, Phys. Rev. E, **93**, 060202 (2016).